Microstructure in a Ternary Microemulsion Studied by Small Angle Neutron Scattering

H. Bagger-Jörgensen,*,† U. Olsson,† and K. Mortensen‡

Physical Chemistry 1, Chemical Center, University of Lund, P.O. Box 124, S-221 00 Lund, Sweden, and Physics Department, Risø National Laboratory, DK-4000 Roskilde, Denmark

Received August 9, 1996. In Final Form: December 2, 1996⊗

The microstructure in a ternary microemulsion, composed of pentaethylene glycol dodecyl ether ($C_{12}E_5$), water, and decane, was investigated by small angle neutron scattering along a dilution line defined by a constant surfactant-to-oil ratio, $\phi_s/\phi_o = 0.815$, where ϕ_s and ϕ_o are the surfactant and oil volume fractions, respectively. In the experiments three different contrasts were applied and the concentration was varied in the range $0.02 \le \phi \le 0.22$, where $\phi = \phi_s + \phi_o$. At lower temperatures the microemulsion phase coexists with excess oil (emulsification failure). Along the emulsification failure phase boundary the results are consistent with a structure of spherical oil droplets, the size of which do not change with concentration. A simultaneous fit to the three different contrasts gives a droplet hydrocarbon radius of $\langle r_{hc} \rangle = 75$ Å and a relative polydispersity $\sigma/r_{hc} = 16\%$. When increasing the temperature, data are consistent with an increase in micellar size and a deviation from spherical shape.

Introduction

Thermodynamically stable mixtures of water, oil and surfactant are generally referred to as microemulsions.[1−3] They are normally transparent, optically isotropic, and of low viscosity. Macroscopically they are homogeneous, but on a microscopic scale they indeed exhibit a certain structure, basically made of a dividing surface, the surfactant layer, separating oil and water from each other. The development of a unifying picture relating the structure and phase equilibria of surfactant−water−oil systems has been the motivation for extraordinary efforts in recent years. For nonionic surfactants it has proven useful to describe the thermodynamics within the flexible surface model.[4−7] Here, the behavior is assumed to be governed by the curvature elasticity of the surfactant film, where the local curvature energy density, expanded to harmonic order, often is written as[8]

$$g_c = 2\kappa(H - H_0)^2 + \bar{\kappa}K \qquad (1)$$

$H = (c_1 + c_2)/2$ and $K = c_1c_2$ are the mean and Gaussian curvatures, respectively, where c_1 and c_2 are the two local principal curvatures. κ and $\bar{\kappa}$ are two modulii, often referred to as the bending and saddle splay modulus, respectively. H_0 is the spontaneous curvature, which for nonionic surfactants of the ethylene oxide type is strongly temperature dependent.[5,9] At lower temperatures the film prefers to curve toward oil and $H_0 > 0$ (where we have defined curvature toward oil as positive). At higher temperatures on the other hand the film has a preferred curvature toward water and $H_0 < 0$. Thus at an intermediate temperature the film has no preference to curve toward either oil or water. This temperature, T_0, where the spontaneous curvature vanishes coincides with the so-called phase inversion temperature (PIT), well-known from emulsion technology.[10] When the spontaneous curvature is near zero (corresponding to temperatures near T_0), a bicontinuous microemulsion, a lamellar phase, and a L_3 (sponge) phase are the three stable phases in the phase diagram, apart from the pure solvents. When H_0 deviates more strongly from zero, a droplet microemulsion is formed. For $H_0 \gg 0$ there is a water-rich phase of oil droplets, and for $H_0 \ll 0$ there is a corresponding oil-rich phase of water droplets. The oil (water) droplets can dissolve a finite amount of oil (water), and the saturated phase coexists with excess oil (water). This coexistence, or incomplete solubilization, has been termed emulsification failure.[11] Another name for the equilibrium, which relates to the pioneering work of Winsor, is Winsor I for the excess oil case and Winsor II for the excess water case. Here, however, we will mainly use the term emulsification failure (EF). At the phase boundary, the flexible surface model predicts, neglecting entropy of mixing, that the droplets are spherical with a radius, r, given by[12]

$$\frac{r}{r_0} = 1 - \frac{\bar{\kappa}}{2\kappa} \qquad (2)$$

where $r_0 \equiv H_0^{-1}$ is the spontaneous radius, i.e. the inverse spontaneous curvature.

Recently, we have investigated a water dilution line in the ternary pentaethylene glycol dodecyl ether ($C_{12}E_5$)−water−decane system for a constant surfactant-to-oil ratio, $\phi_s/\phi_o = 0.815$, where ϕ_s and ϕ_o are the surfactant and oil volume fractions, respectively, with a number of different experimental techniques.[13−16] The T versus ϕ phase

† University of Lund.

‡ Risø National Laboratory.

⊗ Abstract published in *Advance ACS Abstracts,* February 1, 1997.

(1) Schulman, J. H.; Stoeckenius, W.; Prince, L. M. *J. Phys. Chem.* **1959**, *63*, 1677.
(2) Winsor, P. A. *Solvent Properties of Amphiphilic Compounds*; Butterworth: London, 1954.
(3) Hoar, T. P.; Schulman, J. H. *Nature (London)* **1943**, *152*, 102.
(4) Safran, S. A. *Statistical Thermodynamics of Surfaces, Interfaces and Membranes*; Addison-Wesley: Reading, MA, 1994.
(5) Olsson, U.; Wennerström, H. *Adv. Colloid Interface Sci.* **1994**, *49*, 113.
(6) Daicic, J.; Olsson, U.; Wennerström, H. *Langmuir* **1995**, *11*, 2451.
(7) Daicic, J.; Olsson, U.; Wennerström, H.; Jerke, G.; Schurtenberger, P. *J. Phys. II* **1995**, *5*, 199.
(8) Helfrich, W. *Z. Naturforsch.* **1973**, *28c*, 693.
(9) Strey, R. *Colloid Polym. Sci.* **1994**, *272*, 1005.
(10) Shinoda, K.; Friberg, S. E. *Emulsions and Solubilization*; Wiley-Interscience: New York, 1986.
(11) Turkevich, L. A.; Safran, S. A.; Pincus, P. A. In *Surfactants in Solution*; Mittal, K. L., Bothorel, P., Eds.; Plenum Press: New York, 1986; Vol. 6, p 1177.
(12) Safran, S. A. *Phys. Rev. A* **1991**, *43*, 2903.
(13) Leaver, M. S.; Olsson, U. *Langmuir* **1994**, *10*, 3449.
(14) Leaver, M. S.; Olsson, U.; Wennerström, H.; Strey, R. *J. Phys. II* **1994**, *4*, 515.
(15) Leaver, M.; Furo′, I.; Olsson, U. *Langmuir* **1995**, *11*, 1524.
(16) Olsson, U.; Schurtenberger, P. *Langmuir* **1993**, *9*, 3389.

S0743-7463(96)00788-3 CCC: $14.00

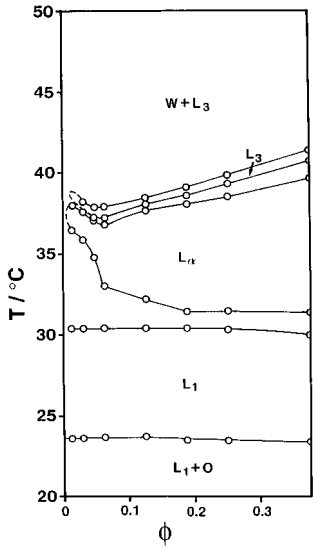

Figure 1. Partial phase diagram of the system $C_{12}E_5$−water−decane (redrawn from ref 16), drawn as volume fraction of surfactant plus oil (ϕ) versus temperature (T). The volume fraction ratio $\phi_s/\phi_o = 0.815$, where ϕ_s and ϕ_o are the surfactant and oil volume fractions, is kept constant. For the various phases the following notations are used: L_1 is a liquid microemulsion phase similar to the normal micellar phase found in binary surfactant−water systems. L_α is a lamellar liquid crystalline phase. L_3 is a liquid phase having a multiply connected bilayer structure. The L_1 phase consists of discrete, oil-swollen droplets covered by a surfactant monolayer close to the lower phase boundary. Curvature is toward oil; i.e., $\langle H \rangle > 0$. The lamellar phase can be described as oil-swollen bilayers stacked with one-dimensional order. Due to the planar topology, $\langle H \rangle = 0$. The L_3 phase consists of a disordered, multiply connected bilayer, which acts as a dividing surface between two separate water labyrinths. While the average mean curvature of the bilayer midplane vanishes by symmetry, the average mean curvature of the surfactant monolayer film is negative, i.e. $\langle H \rangle < 0$.

diagram, where $\phi \equiv \phi_s + \phi_o$, of the water-rich part of this dilution line is reproduced in Figure 1. The water may be either normal H_2O or deuterated water, D_2O (the exchange of H_2O with D_2O only results in a trivial temperature shift of all phase boundaries by approximately 2 °C). With increasing temperature a sequence of three homogeneous phases is obtained: a liquid O/W microemulsion phase (L_1), a lamellar liquid crystalline phase (L_α) and a liquid, bicontinuous phase (L_3). At lower temperatures (<24 °C), the microemulsion phase is in equilibrium with excess (almost pure) oil ($L_1 + O$). The phase changes with temperature reflect the temperature dependence of H_0. For the $C_{12}E_5$ surfactant, this varies approximately linearly with T, $r_0^{-1} = H_0 = \delta(T_0 - T)$, where the temperature coefficient $\delta \approx 10^{-3}$ Å^{-1} K^{-1}.[9,17]

As a complementary investigation of this system, we present in this paper a small angle neutron scattering (SANS) study of the microemulsion phase, as a function of both temperature and concentration. The object is mainly to measure the size, shape, and polydispersity of the micellar aggregates but also to verify the findings obtained previously with other techniques.

Small angle scattering has proven useful in the experimental investigations of microemulsions, providing a suitable q-range for the colloidal dimensions in these systems.[18−20] Recently nonionic microemulsions similar to our system has been studied by SANS.[21−24] In the present study we have, by using both protonated and deuterated decane and water and mixing them in the appropriate amounts, been able to measure different parts of the micellar aggregate. The results will be discussed together with the previous studies on the system, and the advantages and disadvantages with small angle neutron scattering in the study of microemulsions will be discussed.

Experimental Section

Chemicals and Sample Preparation. Pentaethylene glycol dodecyl ether ($C_{12}E_5$) of high quality was obtained from Nikko Chemical Co. Ltd., Tokyo. Decane (99.9%) was purchased from Sigma, and heavy water (D_2O), from Norsk Hydro. The fully deuterated decane ($C_{10}D_{22}$) was obtained from Dr. Glaser AG, Basel. All chemicals were used as received. Samples were prepared 1 week in advance and where thoroughly mixed. Special precaution was needed when preparing the different contrast-matched samples, ensuring that the volume fraction ratio ϕ_s/ϕ_o in all samples was constant. The compositions of the samples containing 2% surfactant + oil, corresponding to $\phi = 0.026$, but with different contrasts (bulk, shell, and core) are, together with their calculated, dry scattering length densities, listed in Table 1. Just before measurement, the solutions were transferred to 1 mm quartz cuvettes. The samples are metastable below the lower phase boundary[14] and, although the room temperature was a few degrees below this boundary, phase separation never occurred.

SANS−Instrumental Setup and Data Treatment. Scattering experiments were performed on the small angle instrument at Risø National Laboratory. Three different detector distances, D, and two different wavelengths, λ, were used. At $\lambda = 12$ Å and $D = 6m$, the q-range was $0.002 < q < 0.02$ Å^{-1}; for $\lambda = 5.6$ Å and $D = 3m$, it was $0.01 < q < 0.1$ Å^{-1}; and for $\lambda = 5.6$ Å, and $D = 1m$, it was $0.02 < q < 0.29$ Å^{-1}. The wavelength spread, $\Delta\lambda/\lambda$, was in all cases 9% (full width at half maximum). The intensity was recorded on a 128 pixel × 128 pixel 2-D detector. All samples gave azimuthally isotropic scattering patterns, and the data were radially averaged. Transmission measurements were done for all samples, setups, and temperatures. The incoherent scattering of H_2O was used for absolute calibration and to take variation in detector response into account. The three absolute scaled parts showed good agreement in overlapping regions (within 10%) and were spliced together with a least squares fit. At the highest q-values the incoherent scattering of the sample dominates, giving rise to a q-independent value. This constant term was subtracted.

The finite instrumental resolution was taken into account by using a previously derived Gaussian resolution function.[25] An advantage with this function is that the different contributions (from wavelength spread, collimation effects, and detector resolution) are simply additive. The measured, radially averaged intensity scattered from a sample with scattering cross section $d\sigma/d\Omega$ is then

$$I(\langle q \rangle) = \int_0^\infty R_{av}(q,\langle q \rangle) \frac{d\sigma(q)}{d\Omega}\, dq \qquad (3)$$

where the resolution function can be approximated by

$$R_{av}(q,\langle q \rangle) = \frac{1}{\sqrt{2\pi}\sigma} \exp\left[-\frac{1}{2}(q - \langle q \rangle)^2/\sigma^2\right] \qquad (4)$$

(17) Rajagopalan, V.; Bagger-Jörgensen, H.; Fukuda, K.; Olsson, U.; Jönsson, B. *Langmuir* **1996**, *12*, 2939.
(18) Chen, S. H. *Annu. Rev. Phys. Chem.* **1986**, *37*, 351.
(19) Cabane, B. In *Surfactant Solutions*; Zana, R., Ed.; Marcel Dekker: New York, 1987; Vol. 22, p 57.
(20) *Neutron, X-Ray and Light Scattering: Introduction to an Investigative Tool for Colloidal and Polymeric Systems*; Lindner, P., Zemb, T., Eds.; North-Holland: Amsterdam, 1991.
(21) Gradzielski, M.; Langevin, D.; Farago, B. *Phys. Rev. E* **1996**, *53*, 3900.
(22) Gradzielski, M.; Langevin, D.; Magid, L.; Strey, R. *J. Phys. Chem.* **1995**, *99*, 13234.
(23) Sicoli, F.; Langevin, D.; Lee, L. T. *J. Chem. Phys.* **1993**, *99*, 4759.
(24) Strey, R.; Glatter, O.; Schubert, K.-V.; Kaler, E. W. *J. Chem. Phys.* **1996**, *105*, 1175.
(25) Pedersen, J. S.; Posselt, D.; Mortensen, K. *J. Appl. Crystallogr.* **1990**, *23*, 321.

Table 1. Sample Compositions and Calculated, Dry Scattering Length Densities for the $\phi = 0.026$ Samples in Shell-, Bulk-, and Core-Contrast

contrast	wt % $C_{12}E_5$	wt % $C_{10}H_{22}$	wt % $C_{10}D_{22}$	wt % H_2O	wt % D_2O	ρ(decane)/10^9 cm^{-2}	$\rho(C_{12}E_5)/10^9$ cm^{-2}	ρ(water)/10^9 cm^{-2}	$\Delta\rho/10^9$ cm^{-2}
shell	1.04	0.034	1.066		97.86	63.2	1.3	64.1	62.8
core	1.04		1.10	87.19	10.67	65.8	1.3	1.3	64.5
bulk	1.04	0.96			98.00	−4.9	1.3	64.1	65.9

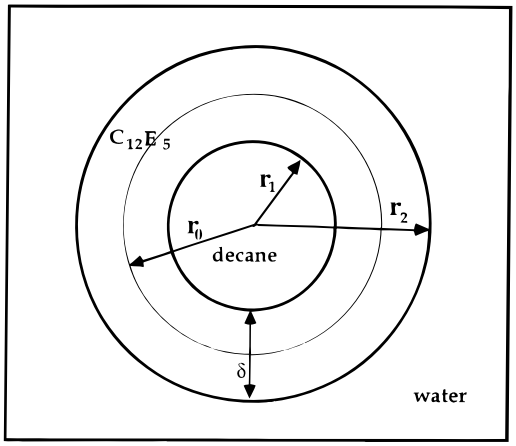

Figure 2. Droplets described as spheres with an inner radius r_1, corresponding to the decane core, and an outer radius r_2. All surfactant molecules are situated in the outer shell. An equivalent description is to use the middle of the surfactant film, r_0, and the shell thickness, $\delta = r_2 - r_1$.

when q is not too small. The variance σ is dependent on $\langle q \rangle$ as well as the instrumental setup.[25]

Theoretical Considerations

Micellar Model. The experimental results will be analyzed using the micellar model illustrated in Figure 2. The aggregates are treated as spheres, covered by a surfactant layer. The oil core has the radius r_1 while the surfactant shell extends out to r_2, thereby defining the outer radius of the micelle. An alternative description is that the center of the film is located at r_0 and that the film thickness is $\delta = r_2 - r_1$. The method of isotopic substitution[19] has been used to extract the maximum amount of information about the aggregate structure. By varying the proton−deuterium ratio of the oil and water, the scattering length density profile can be adjusted to enhance various parts of the micelles. The three different contrasts used here are schematically illustrated in Figure 3. Figure 3a corresponds to decane and $C_{12}E_5$ that are protonated, i.e. a fully protonated aggregate, immersed in deuterated water (D_2O). Since the scattering length densities of $C_{10}H_{22}$ and $C_{12}E_5$ are very similar and much different from the D_2O value, the radial scattering length density is constant from the origin of the micelle up to r_2, as illustrated in the bottom of Figure 3a. The dashed curve corresponds to the diffuse interface model (see next section). To distinguish between the different contrasts we refer to this case as *bulk-contrast*. In Figure 3b the decane is a mixture of protonated and deuterated decane, yielding the same scattering length density as that for D_2O. Here, the neutrons only see the surfactant film, made of protonated $C_{12}E_5$. The radial scattering length density is seen in the bottom of Figure 3b. This situation will in the following be termed *shell-contrast*. The last case, illustrated in Figure 3c, is utilized by mixing protonated and deuterated water to obtain the same contrast as for protonated $C_{12}E_5$. The neutrons only see the micellar core containing deuterated decane. In the bottom of Figure 3c the radial scattering length density is shown. Consequently, we call this *core-contrast*.

SANS. In this section we will summarize relevant information concerning the scattering from an ensemble of spherical droplets. The scattering amplitude, $F(q)$, as a function of the scattering vector, $q = 4\pi/\lambda \sin\theta/2$, where θ is the scattering angle, from a sphere is simply the Fourier transform of its radial scattering length density profile, $\Delta\rho(r) = \rho_{drop}(r) - \rho_{solv}$, i.e.

$$F(q) = \int_V \Delta\rho(r) \exp\{i\vec{q}\vec{r}\}\, dr \tag{5}$$

The form factor, $P(q)$, is the square of the amplitude, i.e. $P(q) = F(q)^2$. For a homogeneous sphere with radius R and the constant scattering length density $\Delta\rho$ (corresponding to bulk-contrast), the form factor is given by

$$P(q)^{sharp}_{bulk} = \Delta\rho^2 V^2 \left(3\frac{j_1(qr)}{qr}\right)^2 \tag{6}$$

where V is the volume of the particle and $j_1(x) = \sin(x)/x^2 - \cos(x)/x$ is the first-order spherical Bessel function. In the case of shell-contrast, where $\Delta\rho(r)$ is constant and equal to $\Delta\rho_{shell}$ between r_1 and r_2 and zero elsewhere, the form factor is

$$P(q)^{sharp}_{shell} = \Delta\rho^2 \left(3V_2\frac{j_1(qr_2)}{qr_2} - 3V_1\frac{j_1(qr_1)}{qr_1}\right)^2 \tag{7}$$

where $V_i = 4\pi r_i^3/3$. The above simple expressions produce satisfying descriptions at lower q ($<2\pi/\delta$). However at higher q, in the so-called Porod regime,[26] the agreement becomes less good. This is due to the fact that the surfactant film is solvated by water and oil on their respective sides of the film. This was pointed out by Strey and co-workers,[22] who also derived the form factor of a "diffuse" spherical shell, assuming a Gaussian scattering length density profile

$$\rho(r) = \Delta\rho \exp\{-(r - r_0)/2t^2\} \tag{8}$$

centered in the middle of the surfactant film at r_0, with a thickness parameter t and the maximum value of $\Delta\rho$. This type of profile will in the following be termed the *diffuse interface model* to distinguish it from the earlier described *sharp interface model* (see Figure 3). The scattering amplitude for the shell-contrast case is readily calculated using eq 5, yielding[22]

$$F^{diffuse}_{shell}(q) = \Delta\rho\frac{4\pi\delta}{q}\exp\left\{-\frac{q^2t^2}{2}\right\}(r_0 \sin qr_0 + qt^2 \cos qr_0) \tag{9}$$

where δ is the corresponding shell thickness in the sharp interface model. δ and t are related through

$$t = \frac{\delta}{\sqrt{2\pi}}\frac{r_0^2 + \delta^2/12}{r_0^2 + t^2} \approx \frac{\delta}{\sqrt{2\pi}} \tag{10}$$

ensuring that the amount of scattering material is the same in the two models.

The scattering amplitude from a sphere with a diffuse interface in bulk contrast may be calculated in a similar way. The radial scattering length density is here

$$\rho(r) = \begin{cases} \Delta\rho & 0 \le r \le r_0 \\ \Delta\rho \exp\left\{-\dfrac{(r - r_0)^2}{2t^2}\right\} & r \ge r_0 \end{cases} \tag{11}$$

(26) Porod, G. In *Small Angle X-ray Scattering*; Glatter, O., Kratky, O., Eds.; Academic Press: New York, 1982.

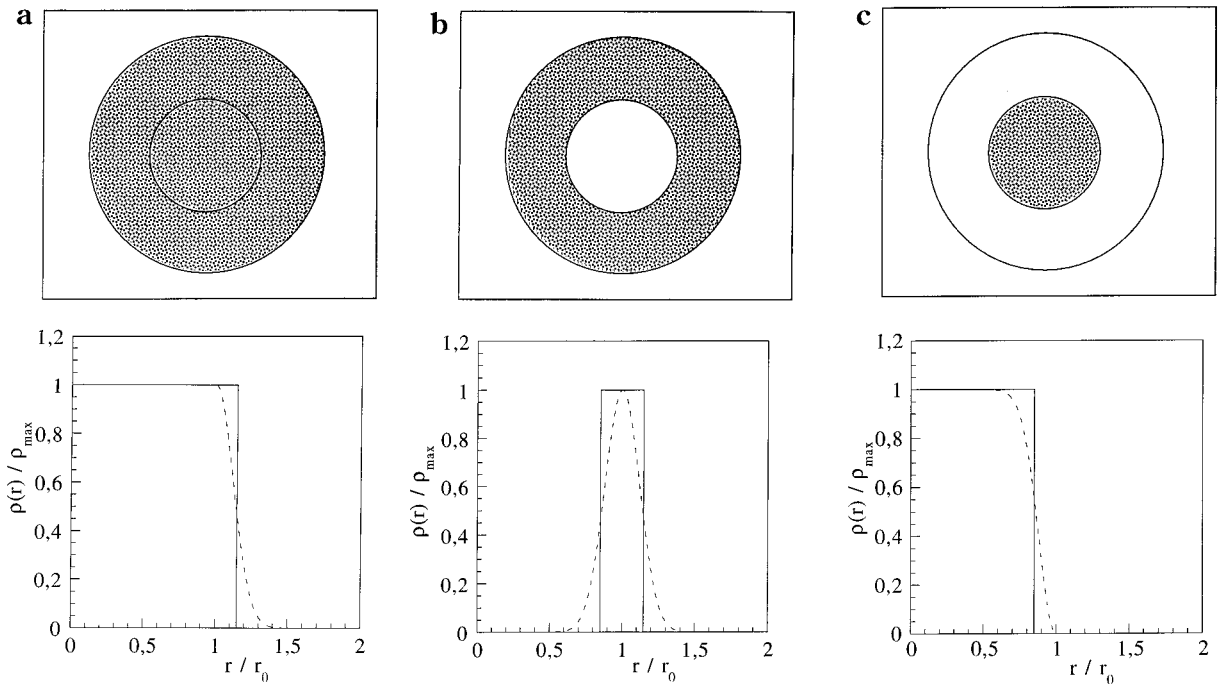

Figure 3. Illustration of the contrast variation technique (top). With protonated decane and $C_{12}E_5$ and deuterated water, we measure with *bulk-contrast*, illustrated in part a. The corresponding radial density is drawn just below. The full line corresponds to the sharp interface model, while the dashed curve is a diffuse interface, allowing for decane and water penetration into the surfactant film. (b) With deuterated decane and water and protonated $C_{12}E_5$, we measure with *shell-contrast*. (c) We get *core-contrast* by using deuterated decane and protonated $C_{12}E_5$ and water.

Inserting this $\rho(r)$ into eq 5 yields

$$F_{\text{bulk}}^{\text{diffuse}}(q) = \Delta\rho\frac{4\pi}{q}\left[r_0^2 j_1(qr_0) + t^2\sin(qr_0) + \sqrt{\frac{\pi}{2}}\exp\left[-\frac{(qt)^2}{2}\right]\left\{qt^3\cos(qt) + r_0 t\sin(qr_0) + \text{erf}\left[\frac{tq}{\sqrt{2}}\right](qt^3\sin(qr_0) + r_0 t\cos(qr_0))\right\}\right] \quad (12)$$

where $\text{erf}(x) = 2/\sqrt{\pi}\int_0^x e^{-t^2}$ is the error integral.

The corresponding r_2 in the sharp interface model is $r_2 = r_0 + \delta/2$, where δ is calculated by applying eq 10.

In the polydisperse case the intensity is calculated by integrating the form factors of all radii, $P(q,r)$, weighted by a size distribution function $f(r)$

$$P(q,r_{\text{mean}}) = \int P(q,r)\, f(r)\, dr \quad (13)$$

The resolution generally does not allow for an explicit determination of the size distribution, and it is then, for simplicity, often assumed to be Gaussian, with a mean value at r_0 and a variance σ. The integral in eq 13 has an analytical solution for the diffuse interface model with shell-contrast[22] (the expression is rather long and is not reproduced here) but to our knowledge not in the other cases. The integration of eq 13 was therefore performed numerically for the other contrast profiles.

The surfactant film is penetrated by both oil and water. For the case of shell-contrast this implies that the maximum in $\rho(r)$ does not necessarily equal the full scattering length density difference between the surfactant and the solvents, $\rho_s - \rho_w = \rho_s - \rho_o$ but may have a smaller value. The mean inner volume of the droplet, containing decane, may in the polydisperse case be written

$$\bar{V}_{\text{decane}} = \frac{4\pi}{3}\left\{r_0(r_0^2 + 3\sigma^2) - \frac{3}{2}\delta(r_0^2 + \sigma^2) + \frac{3}{4}r_0\delta^2 - \frac{1}{8}\delta^3\right\} \quad (14)$$

and correspondingly for the volume of the surfactant shell

$$\bar{V}_{\text{shell}}^{\text{wet}} = 4\pi\delta(r_0^2 + \sigma^2) \quad (15)$$

where the index "wet" here reminds that this volume also includes the penetrating oil and water. Since we have a fixed volume fraction ratio, ϕ_s/ϕ_o, we may also identify a "dry" shell volume, containing only surfactant, by

$$\bar{V}_{\text{shell}}^{\text{dry}} = \bar{V}_{\text{decane}}\frac{\phi_s}{\phi_o} \quad (16)$$

The scattering length density, when oil and water are penetrating the film, is defined by

$$\Delta\rho_{\text{shell}}^{\text{wet}} = \frac{\bar{V}_{\text{shell}}^{\text{dry}}}{\bar{V}_{\text{shell}}^{\text{wet}}}\Delta\rho_{\text{shell}}^{\text{dry}} \quad (17)$$

where $\Delta\rho_{\text{shell}}^{\text{dry}}$ is the value calculated from the individual atomic scattering lengths and the surfactant volume.

In the general case we also have to take the droplet−droplet interaction into account. For monodisperse spheres the intensity, $I(q)$, may be written as a product of the number density of micelles, $N = \phi_s/V_{\text{shell,dry}}$, the form factor, $P(q)$, and a structure factor, $S(q)$, i.e.

$$I(q) = NP(q)\, S(q) \quad (18)$$

The structure factor contains information about the interdroplet interaction. In the polydisperse case the factorization of $P(q)$ and $S(q)$ is not strictly valid.[27] However, if the polydispersity is low, eq 18 has been proven empirically useful. Explicit calculations of the structure factor are difficult. Simple, analytical expressions are available only in a few cases, such as, for example for monodisperse particles interacting as hard spheres, the so-called Percus−Yevick expression.[28,29] In the limit of zero scattering vector a simple and very accurate relation between $S(q=0)$ and the hard sphere volume fraction of particles, ϕ_{HS}, is

(27) Robertus, C.; Philipse, W. H.; Joosten, J. G. H.; Levine, Y. K. *J. Chem. Phys.* **1989**, *90*, 4482.
(28) Percus, J. K.; Yevick, G. J. *Phys. Rev.* **1958**, *110*, 1.
(29) Ashcroft, N. W.; Lekner, J. *Phys. Rev.* **1966**, *145*, 83.

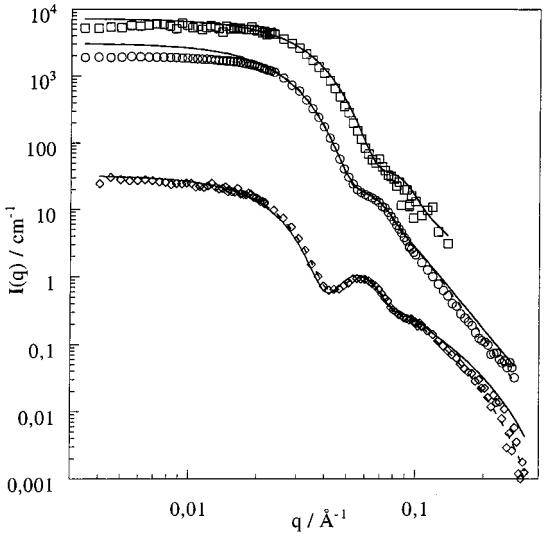

Figure 4. The experimental scattering at 24 °C from the $\phi = 0.026$ sample with three different contrasts: shell (◇), bulk (○), and core (□). Note that the bulk and core curves have, for clarity, been multiplied by a factor of 10 and 100, respectively. The experimental data from all three sets were simultaneously fitted to the sharp interface model (solid line) and the diffuse interface model (dashed line). The fit yielded an average hydrocarbon radius $r_0 = 68 \pm 1$ Å, a relative polydispersity $\sigma/r_0 = 0.16$, and a surfactant shell thickness $\delta = 15 \pm 0.5$ Å. The two models produce almost identical results at low and intermediate q-values, whereas the behavior at high q-values is quite different. In this region the diffuse interface model describes the experimental scattering best.

also known, the Carnahan−Starling expression[30]

$$S_{CS}(0) = \frac{(1 - \phi_{HS})^4}{(1 + 2\phi_{HS})^2 - \phi_{HS}{}^3(4 - \phi_{HS})} \qquad (19)$$

The general features of $S(q)$ are however that, for sufficiently dilute solutions, it reaches unity. Also for moderate concentrations and at $q \gg \pi/R_{mic}$ it reaches 1. Therefore, the measured intensity can be fitted to the formfactor $P(q)$ if the intensity at low q-values is omitted from the fit.

Results

Along the EF Boundary. In this section we will present the results from the most dilute samples, $\phi = 0.026$, measured with the three contrasts described in the previous section, namely the shell-, bulk-, and core-contrasts. We will also compare the sharp interface model and the diffuse interface model with the scattering data. The scatterings for all three contrasts are shown in Figure 4. With shell-contrast (bottom) the most characteristic spectrum is seen, with two distinct dips reminiscent of the Bessel oscillations. The radius and polydispersity may be extracted with high accuracy. The bulk-contrast sample (middle) shows only one shallow dip. Still, the data fitting is fairly accurate. The core-contrast sample (top) has a high incoherent background, since the water in this case was protonated (the incoherent scattering comes almost exclusively from protons). The relatively high background made the coherent intensity afflicted with large error bars already at $q \approx 0.1$ Å^{-1}, making data fitting less accurate. The three spectra were simultaneously fitted to the earlier described form factors (see section 3), both in the sharp and the diffuse interface model. The scattering length densities were calculated from the atomic scattering lengths and the respective molecular volumes, giving $\Delta\rho^{dry}_{bulk} = 6.5 \times 10^{10}$ cm^{-2}, $\Delta\rho^{dry}_{core} = 6.4 \times 10^{10}$ cm^{-2}, and $\Delta\rho^{dry}_{shell} = 6.2 \times 10^{10}$ cm^{-2}. Three independent parameters were extracted from the fit; the mean radius r_0, the shell thickness δ (equivalently r_1 and r_2), and the polydispersity σ/r_0. The calculated scattering length densities for the bulk- and core-contrasts are in good agreement with experiment, while for the shell-contrast the fitted (i.e. derived from the fitted parameters using eq 17) $\Delta\rho^{wet}_{shell} = 5.4 \times 10^{10}$ cm^{-2} is more than 10% lower than the calculated, dry value. Thus, the surfactant film is to a significant degree penetrated by water and decane and the maximum scattering length density never reaches the calculated value for pure surfactant.

(30) Carnahan, N. F.; Starling, K. E. *J. Chem. Phys.* **1969**, *51*, 635.

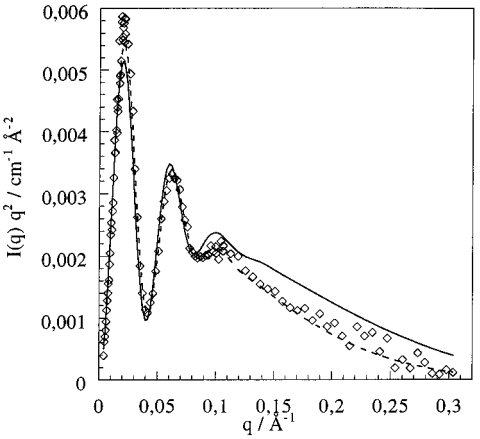

Figure 5. Same data as in Figure 4 (drawn as Iq^2 versus q) except that only the shell-contrast sample is shown. Note the good agreement between the experimental and the calculated curves.

As seen from the fits in Figure 4, both the sharp interface model (solid line) and the diffuse interface model (broken line) satisfactorily describe the experimental scattering (except perhaps at the highest q-values, where the data are strongly sensitive to the incoherent background), with the parameters $r_0 = 68$ Å, $\delta = 15$ Å, and $\sigma/r_0 = 0.16$. At high q-values the diffuse interface model follows the experimental data better than the sharp interface model, in accordance with earlier observations.[22] The quality of the fit is best seen in Figure 5, drawn as Iq^2 versus q. Only the shell-contrast data and the corresponding fitted curves are shown. Obviously the diffuse interface model gives the best description of the experimental data. It appears that the shell-contrast sample most clearly reveals structural information, and hence this contrast was used in the following concentration and temperature study.

Moving along the emulsification failure at 24 °C, toward increasing concentration, the scattered intensities were recorded also at $\phi = 0.065$, $\phi = 0.13$, and $\phi = 0.25$ with shell-contrast. The resulting scattering curves, normalized by dividing by the volume fraction of surfactant, are shown in Figure 6a (drawn as log(I) versus log(q)) and Figure 6b (drawn as Iq^2 versus q). From the exact correspondence at high q-values ($q > 0.03$ Å^{-1}) it is clear that the form factor is identical in all three cases; i.e., the micellar dimension is invariant as a function of concentration along the EF boundary. The mismatch we see at low q-values is due to interaction between the micelles, showing that we must include a structure factor in our analysis.

We now turn to examine the interparticle interaction. According to eq 20 we may, if the form factor is known, obtain the structure factor simply by dividing the intensity by $P(q)$. This operation is slightly hazardous, since we know we have a polydisperse system. We may however define the average structure factor,[27] $\tilde{S}(q)$, to distinguish

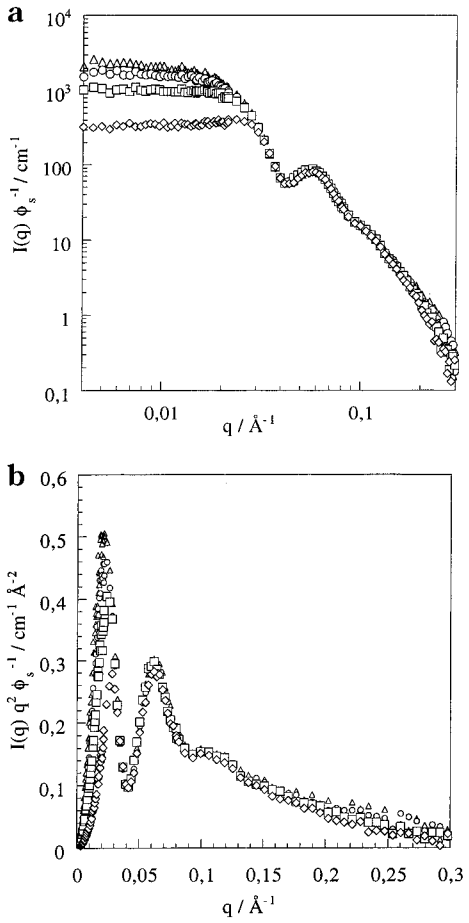

Figure 6. Superposition of experimental scattering from the $\phi = 0.026$ (△), $\phi = 0.065$ (○), $\phi = 0.13$ (□), and $\phi = 0.25$ (◇) samples with shell-contrast at 24 °C (close to EF). The intensities have been normalized by dividing by the surfactant volume fraction. The curves are, within experimental error, identical for $q > 0.03$ Å^{-1}, showing that the form factor, and thereby the micellar dimension, is invariant as a function of concentration at this temperature. The mismatch at low q-values is due to intermicellar interaction (i.e. $S(q) \neq 1$). In part a the data are shown in a double logarithmic plot while in part b Iq^2 versus q is shown in a linear plot.

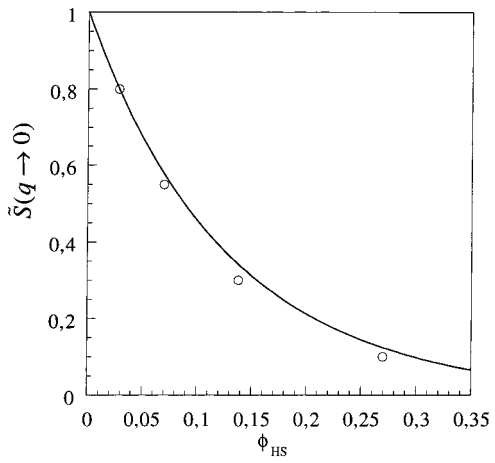

Figure 7. Average structure factor extrapolated to zero scattering vector, $S(q \rightarrow 0)$, (○) as a function of ϕ. The solid line is $S_{CS}(0)$ calculated with the Carnahan−Starling expression, eq 19. The hard sphere volume fraction was $\phi_{HS} = 1.14\phi$, taken from ref 16.

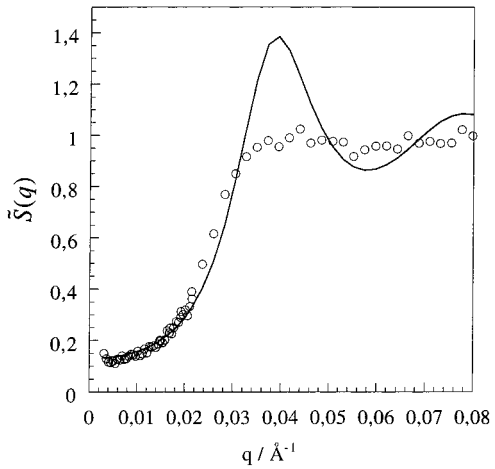

Figure 8. Average structure factor $\bar{S}(q)$, calculated according to eq 20, (○) for $\phi = 0.25$ with shell-contrast at 24 °C. For comparison the Percus−Yevick structure factor for monodisperse hard spheres ($R_{HS} = 80$ Å) is shown as a solid line.

from the strict thermodynamic $S(q)$, i.e.

$$\tilde{S}(q) \equiv \frac{I(q)}{NP(q)} \tag{20}$$

First we compare $\tilde{S}(0)$ with the Carnahan−Starling expression for hard spheres, eq 19. The hard sphere volume fraction, ϕ_{HS}, was in an earlier study found to be 14% larger than the volume fraction of surfactant and oil,[16] i.e. $\phi_{HS} = 1.14\phi$. The experimental $\tilde{S}(q \rightarrow 0)$ and the calculated $S_{CS}(0)$ as a function of concentration are presented in Figure 7. As seen from the figure, the correspondence between the experimental $\tilde{S}(q \rightarrow 0)$ and the calculated $S_{CS}(0)$ is, within experimental error, good. It is interesting to compare the measured $\tilde{S}(q)$ with the P−Y expression for hard spheres, since Figure 7 and a previous study[16] indicate that the micelles indeed interact as hard spheres. In Figure 8 this comparison is made for the most concentrated sample, $\phi = 0.25$. The experimental and theoretical curves look rather different, except for their values close to $q = 0$. The experimental $\tilde{S}(q)$ shows a monotonic increase as a function of q until it reaches its limiting value, unity. The calculated $S_{P-Y}(q)$ on the other hand shows an oscillating behavior before reaching unity. The discrepancy may be due to several factors. The simplest explanation is that the droplets do not have a pair potential that exactly resembles that of hard spheres. However, this is a rash conclusion, since the P−Y expression is valid only in the monodisperse case and, although numerical calculations have shown[31] that a polydispersity with this magnitude would not substantially alter the shape of the structure factor, an exact correspondence is not to be expected. Shape polydispersity may have an even more severe effect on the structure factor. Hence, we may conclude this section by stating that the micelles appear to interact as monodisperse hard spheres when studying $\tilde{S}(q \rightarrow 0)$, but when the complete, average structure factor $\tilde{S}(q)$ is studied, it is obvious that the case is not that simple.

Temperature Dependence. We now present the temperature dependence of the microstructure in the microemulsion phase. The four samples examined along the lower phase boundary were also studied at 26, 28, and 30 °C, i.e. through the whole microemulsion phase. The result from the $\phi = 0.026$ sample is shown in Figure 9a (drawn as Iq^2 versus q). The form factor remains essentially the same up to 28 °C, whereas a slight change is seen at 30 °C. With the most concentrated sample, $\phi = 0.25$, (Figure 9b) the structural change starts already

(31) Beurten, P. v.; Vrij, A. *J. Chem. Phys.* **1981**, *74*, 2744.

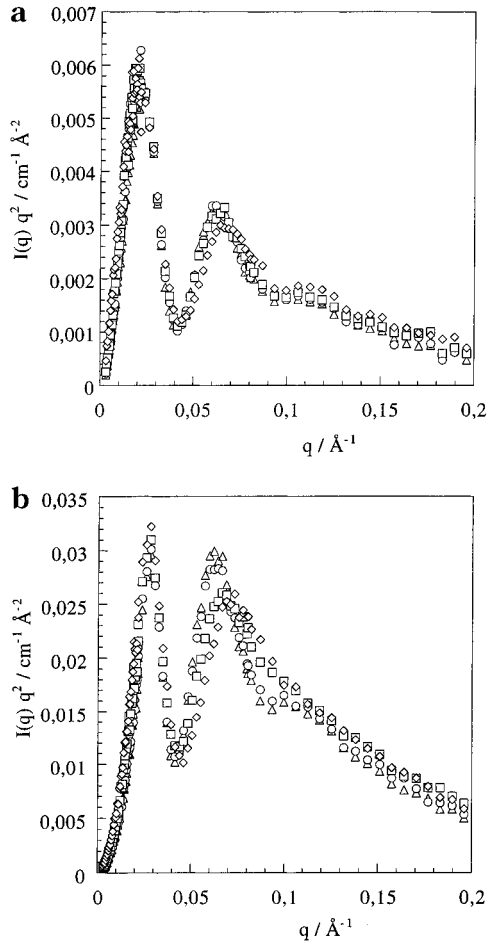

Figure 9. (a) Superposition of the experimental intensities for the $\phi = 0.026$ sample with shell-contrast at 24 (△), 26 (○), 28 (□), and 30 °C (◇). (b) Superposition of the experimental intensities for the $\phi = 0.25$ sample with shell-contrast at 24 (△), 26 (○), 28 (□), and 30 °C (◇).

Table 2. Fitted Micellar Hydrocarbon Radius r_0 and Relative Polydispersity σ/r_0 for Different Concentrations and Temperatures

conc (ϕ)	temp (°C)	r_0/Å	σ/r_0
0.026	24	68	16
0.065	24	68	16
0.13	24	68	16
0.25	24	68	16
0.026	26	68	16
0.065	26	68	16
0.13	26	68	16
0.25	26	67	18
0.026	28	68	16
0.065	28	68	16
0.13	28	66	19
0.25	28	≈60	≈24
0.026	30	65	18
0.065	30	63	20
0.13	30	≈60	≈22
0.25	30	≈56	≈24

at 26 °C and is very pronounced at 28 and 30 °C. The fitted parameters from all samples and temperatures (r_0 and σ/r_0) are given in Table 2. In three cases the agreement between experimental and calculated curves was less good and the fitted parameters were somewhat unsure; in these cases we have put a "≈" before the fitted parameter.

Discussion

It has been experimentally established with $C_{12}E_5$[17,32,33] that the polar−apolar interface, separating the pentaethylene oxide from the hydrocarbon chain of the surfactant monolayer, has an essentially invariant area per molecule, thus behaving as a so-called neutral surface. The hydrocarbon radius of the (monodisperse) spherical micelles, related to that interface, can be calculated from

$$r_{hc} = \frac{3\left(\Phi_o + \frac{1}{2}\Phi_s\right) l_s}{\Phi_s} \tag{21}$$

where we note that the polar−apolar interface encloses the oil and the hydrocarbon tail of the surfactant, the latter corresponding to approximately half of the surfactant volume, v_s. l_s is the surfactant length, defined as $l_s \equiv v_s/a_s$, where $v_s = 702$ Å^3 [33] is the surfactant volume and a_s is the area per molecule at the polar−apolar interface.

Along the EF boundary we get a micellar dimension that is independent of concentration in the studied interval. All three contrasts give exactly the same micellar radius, measured at the polar−apolar interface, $r_{hc} = 68$Å, and the same relative polydispersity, $\sigma/r_{hc} = 0.16$. The obtained radius is the first moment of the size distribution. Another way of defining the radius of the droplet would be in analogy with eq 21 writing it as the ratio between the mean hydrocarbon volume and area

$$\langle r_{hc} \rangle = \frac{3\langle V_{hc} \rangle}{\langle A_{hc} \rangle} = \frac{\int r^3 f(r)\, dr}{\int r^2 f(r)\, dr} \tag{22}$$

i.e. as the ratio between the third and second moments of the size distribution. With this definition we measure a mean hydrocarbon radius of $\langle r_{hc} \rangle = 75$ Å. The average area per surfactant, a_s, is not used as a fitting parameter, since it is related to the other parameter through

$$a_s = \frac{\bar{A}_{shell}}{\bar{V}_{decane}} \frac{\phi_o}{\phi_s} v_s \tag{23}$$

where $\bar{A}_{shell} = 4\pi(r_0^2 + \sigma^2)$. Independent of the way we express the mean radius we obtain a surfactant length $l_s \equiv v_s/a_s$ of 14.5 Å, calculated according to eqs 21 or 23, a value which is in good agreement with those of other studies.[14,16,17,33−35] This is satisfactory and tells us that the analysis is correct. Comparing the diffuse and sharp interface models, it is found that the diffuse interface model describes the scattering at high q-values more correctly than the sharp interface model, but they yield identical values of the radius and the polydispersity.

The effect of solvent penetration is observed as a deviation from the classical Porod law[26] at high q and from analyzing the absolute scaled intensity with shell contrast. In the latter case, an approximately 10% lower $\Delta\rho$ is observed compared to the full scattering length density difference between pure surfactant and solvent. This difference is important, since the scattered intensity scales as $\Delta\rho^2$. When a full contrast between surfactant and solvent is assumed,[22,36] this results in a too large area per surfactant molecule when analyzed from the absolute scaled intensity.

The droplet polydispersity is a complex problem involving a distribution in both the surfactant, n_s, and oil, n_o, aggregation numbers, leading to a distribution both in

(32) Leaver, M. S.; Olsson, U.; Wennerström, H.; Strey, R.; Wurz, U. *J. Chem. Soc., Faraday Trans.* **1994**, *91*, 4269.
(33) Olsson, U.; Würz, U.; Strey, R. *J. Phys. Chem.* **1993**, *97*, 4535.
(34) Strey, R.; Schomäcker, R.; Roux, D.; Nallet, F.; Olsson, U. *J. Chem. Soc., Faraday Trans.* **1990**, *86*, 2253.
(35) Fukuda, K.; Olsson, U.; Würz, U. *Langmuir* **1994**, *10*, 3222.
(36) Strey, R.; Winkler, J.; Magid, L. *J. Phys. Chem.* **1991**, *95*, 7502.

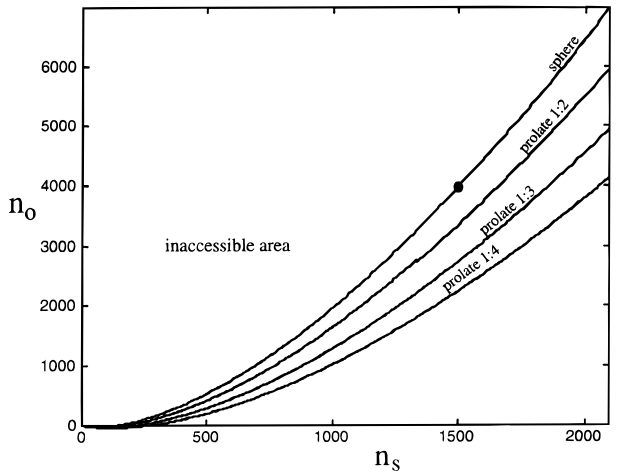

Figure 10. Possible aggregate shapes as a function of the number of oil, n_o, and surfactant, n_s, molecules, calculated for a constant surfactant headgroup area, a_s = 48 Å^2. The distribution in the (n_s, n_o) plane is limited to the high n_s side of a line representing the limiting spherical shape (minimum area for a given volume). Higher n_s values (for a given n_o) correspond to nonspherical shapes, in the figure exemplified by prolates with axial ratios 1:2, 1:3, and 1:4. The filled circle on the sphere line represents the mean aggregate dimension in our system.

size (volume) and shape. For a constant area per surfactant molecule at the polar−apolar interface (or a constant average surfactant area within each droplet) the distribution in the (n_s, n_o) plane is limited to the high n_s side of a line representing the limiting spherical shape (minimum area for a given volume). In Figure 10, this line has been calculated for an area per $C_{12}E_5$ molecule of 48 Å^2 at the previously defined polar−apolar interface separating the alkyl block from the ethylene oxide block of the surfactant. (n_s, n_o) combinations on the high n_s side of the limiting sphere line correspond to nonspherical shapes with a larger deviation from a sphere the higher the n_s value (for a given n_o). This is illustrated in Figure 10, where we also have calculated some lines of constant axial ratio prolate shapes. In our data analysis we only consider a distribution of aggregates along the sphere line. A complementary way to study the polydispersity is to perform a contrast variation experiment, monitoring the forward scattering, $I(0)$.[37,38] Such an experiment, which essentially probes volume polydispersity, has recently been performed on a system similar to ours.[21] If the variation in the structure factor around the match point is properly taken into account,[39] this experiment seems to indicate that the volume polydispersity is significantly smaller than the polydispersity evaluated from the full form factor, assuming a spherical radius polydispersity only, in other words suggesting a significant contribution to the form factor polydispersity origin from shape polydispersity. A similar conclusion was also reached by Ricka et al.[38] for a reverse micellar system. However further experiments along these lines are needed to clarify the issue.

With the preceding polydispersity discussion in mind we seek an interpretation of the results obtained when the temperature is increased. For all concentrations the spectra change when the temperature is enhanced. At low concentration the change is very small, but at ϕ = 0.13 and ϕ = 0.25 a marked increase in polydispersity and also a decrease in mean radius is detected (see Table 2).

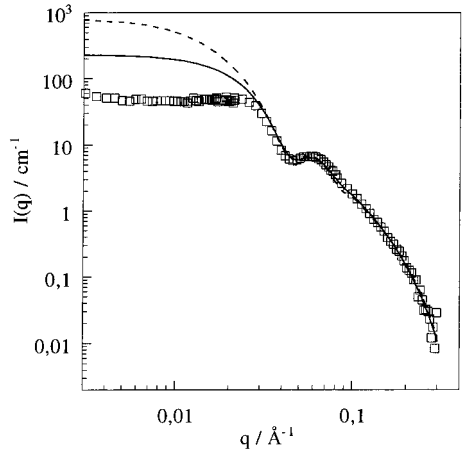

Figure 11. Scattered intensity for the ϕ = 0.026 sample at 28 °C (□), the calculated form factor for a prolate with an axial ratio 1:3, a polydispersity of 13%, and the same area-to-enclosed-volume as for spheres (solid line) and the fitted spherical form factor with radius r_0 = 60 Å and a polydispersity of 24% (broken line). The two calculated form factors are very similar at high q-values, while they deviate at low q-values. Since the structure factor is unknown, it is not possible to distinguish the two possible models.

In fact, at 30 °C we are not able to get a reasonable fit using a spherical form factor. It is at this point informative to compare with a previous NMR relaxation and self-diffusion study[14,15] on the same microemulsion system, focusing on micellar growth. It was shown that dilute samples (ϕ < 0.05) had a very limited growth upon increasing the temperature above EF, while more concentrated samples (ϕ > 0.10) showed a substantial growth already a few degrees above EF and finally, around 30 °C, formed a bicontinuous structure. Analyzing the particle growth in terms of prolates, the axial ratio at ϕ = 0.25 and 28 °C was found to be around 1:3. In Figure 11 the scattered intensity from the ϕ = 0.25 sample is shown, together with the calculated form factor for a prolate with an axial ratio 1:3, a polydispersity of 13%, and the same area-to-enclosed-volume as for spheres (solid line). For comparison the fitted spherical form factor with radius r_0 = 60 Å and σ/r_0 = 0.24 (broken line) is shown. The two calculated curves are very similar at high q-values and, although the axial ratio is as high as 1:3, it is not possible to unambiguously discriminate the two cases, since the structure factor is unknown. However, the scattering data are consistent with the relaxation study. For the highest temperature (30 °C) and concentrations (ϕ = 0.13 and ϕ = 0.25), the fit of a spherical form factor to the experimental intensity was less successful. This is not surprising, since it is clearly seen from self-diffusion data that these samples are bicontinuous.[14]

The micellar growth with increasing temperature and also the formation of a lamellar phase with essentially infinite aggregation at elevated temperatures are a general properties of nonionic surfactants. Since entropy rather favors smaller aggregates, it follows that the growth with increasing temperature is driven by energy. In fact, a growth from spheres into cylinders and further into lamellae is predicted as a function of decreasing spontaneous curvature.[11] The growth in the present system involves only small axial ratios as opposed to binary systems, where when growth occurs, micelles may grow very fast with increasing concentration. The difference is that, in the present three-component system, the spherical micelle is already a very large aggregate containing approximately 5000 surfactant and oil molecules, as compared to an aggregation number of <100

(37) Christ, S.; Schurtenberger, P. *J. Phys. Chem.* **1994**, *98*, 12708.
(38) Ricka, J.; Borkovec, M.; Hofmeier, U. *J. Chem. Phys.* **1991**, *94*, 8503.
(39) Yan, Y. D.; Clarke, J. H. R. *J. Chem. Phys.* **1990**, *93*, 4501.

for a pure surfactant spherical micelle. As a consequence, the number density of micelles is low and the growth is limited by the entropy of mixing.

We finally stress the importance of combining small angle neutron scattering experiments with other experimental techniques. Obviously, SANS is one of the best experimental techniques to measure the size and polydispersity of nearly spherical particles. However, small angle scattering has certain limitations. For instance is it impossible to unambiguously distinguish between polydisperse spheres and monodisperse particles with another shape, such as, for example, prolates; the oscillations in the form factor may be well described by both models.[40] In our case, without comparing with earlier NMR relaxation and self-diffusion studies, the actual aggregate growth might have been misinterpreted as a decrease in micellar size. Also the structural change from discrete micelles to a bicontinuous structure is almost impossible to detect with SANS, whereas the transition is marked in a self-diffusion experiment.

Acknowledgment. This work was supported by the Swedish Natural Science Research Council (NFR). Helpful discussions with Peter Schurtenberger are kindly acknowledged.

LA960788S

(40) Hayter, J. B. In *Physics of Amphifiles: Micelles, Vesicles and Microemulsions*; Digiorgio, V., Corti, M., Eds.; North-Holland: Amsterdam, 1985; p 59.